Photoionization and transient Wannier-Stark ladder in silicon: First principle simulations versus Keldysh theory. Supplemental Material

Thibault J.-Y. Derrien,[1,*] Nicolas Tancogne-Dejean,[2] Vladimir P. Zhukov,[1,3] Heiko Appel,[2] Angel Rubio,[2] and Nadezhda M. Bulgakova[1,†]

[1] *HiLASE Centre, Institute of Physics, Academy of Science of the Czech Republic, Za Radnicí 828/5, 25241 Dolní Břežany, Czech Republic*

[2] *Max Planck Institute for the Structure and Dynamics of Matter (MPSD), Luruper Chaussee 149, 22761 Hamburg, Germany*

[3] *Federal Research Center for Information and Computational Technologies, 6 Lavrentyev Ave., 630090 Novosibirsk, Russia*

I. DETAILS OF THE NUMERICAL APPROACH

A. Time-dependent Kohn-Sham equation

The electrons in the crystal are modeled using the Kohn-Sham (KS) auxiliary system that provides a one-to-one correspondence of the total electron density $n_{\mathrm{e}}(\boldsymbol{r},t)$ of the N non-interacting electrons with the electron density of the many-body problem.[1,2] We solve the time-dependent KS equations for the diamond structure of Si crystal along with applying periodic boundary conditions in all directions. The dynamics of the N electrons in the crystal is described by solving a set of N KS equations, expressed by[3]

$$\left[\left(-\frac{i\hbar}{2m_e}\boldsymbol{\nabla}_{\boldsymbol{r}}+\frac{|e|}{c}\boldsymbol{A}(t)\right)^2+\hat{v}_{\mathrm{ion}}(\boldsymbol{r})+\hat{v}_{\mathrm{H}}[n_{\mathrm{e}}(\boldsymbol{r},t)](\boldsymbol{r})+\right. \tag{1}$$
$$\left.+\hat{v}_{\mathrm{xc}}[n_{\mathrm{e}}(\boldsymbol{r},t)](\boldsymbol{r})\right]\times\psi_{n,\boldsymbol{k}}(\boldsymbol{r},t)=i\hbar\frac{\partial}{\partial t}\psi_{n,\boldsymbol{k}}(\boldsymbol{r},t)$$

where $\boldsymbol{\nabla}_{\boldsymbol{r}}$ describes the real-space gradient operator, $\hbar$ is the reduced Planck constant, m_e is the bare electron mass, $|e|$ is the elementary charge, and c is the light velocity in vacuum. Note that the non-local contribution of the pseudo-potential to the external potential has been omitted for simplicity. $\hat{v}_{\mathrm{ion}}$ is the ionic potential, $\hat{v}_{\mathrm{H}}$ is the Hartree potential, $n_{\mathrm{e}}(\boldsymbol{r},t)$ is the *total* density of electrons (i.e., all electrons in the valence and conduction bands) at the position $\boldsymbol{r}$ and instant t, and $\hat{v}_{\mathrm{xc}}$ is the exchange-correlation potential. $\psi_{n,\boldsymbol{k}}(\boldsymbol{r},t)$ is the time-dependent KS wave-function of an electron located in a band n with a wave-vector $\boldsymbol{k}$. The external vector field $\boldsymbol{A}(t)$ is introduced in the velocity gauge and is taken homogeneous in the simulation volume (dipolar approximation, see Ref.[4]). The ground-state KS wave-function $\psi^{\mathrm{GS}}_{n,\boldsymbol{k}}(\boldsymbol{r})$ is obtained by solving self-consistently the static KS equations.[4] The ground state band structure is given by the energy representation of the eigenvalues $\varepsilon_{n,\boldsymbol{k}}$ as a function of $\boldsymbol{k}$ taken along the path of high-symmetry points for Si crystal.

B. Calculations of the excited electron density

The excited electron density $n_{\mathrm{exc}}(\boldsymbol{r},t)$ evolving in the conduction bands can be evaluated by a projection of the occupied time-evolved KS orbitals $\psi_{n',\boldsymbol{k}}(\boldsymbol{r},t)$ on the ground state KS orbitals $\psi^{\mathrm{GS}}_{n,\boldsymbol{k}}(\boldsymbol{r})$ expressed by[5,6]

$$n_{\mathrm{exc}}(t)=\frac{1}{V}\left[N_{\mathrm{tot}}-\sum_{n,n',\boldsymbol{k}}^{\mathrm{occ.}}\left|\int d^3\boldsymbol{r}\,\psi^{*}_{n',\boldsymbol{k}}(\boldsymbol{r},t)\,\psi^{\mathrm{GS}}_{n,\boldsymbol{k}}(\boldsymbol{r})\right|^2\right]. \tag{2}$$

V is the volume of the simulation box (constant in this work). N_{tot} is the total number of electrons in the simulation box, expressed by $N_{\mathrm{tot}}=\sum_{n,\boldsymbol{k}}\left|\psi^{\mathrm{GS}}_{n,\boldsymbol{k}}(\boldsymbol{r})\right|^2$. Note that initially electrons are absent in the conduction bands.

C. TDDFT calculations of the excitation rates w_{PI}

To avoid the gauge-dependence during the laser pulse, we use the results obtained by the end of the laser pulse of duration τ_p, and define a pulse-averaged excitation rate $w^{\mathrm{TDDFT}}_{\mathrm{PI}}$ based on the density of excited electrons, expressed via

$$w^{\mathrm{TDDFT}}_{\mathrm{PI}}=\frac{n_{\mathrm{exc}}(t=\tau_p)-n_{\mathrm{exc}}(t=0)}{\tau_p}. \tag{3}$$

$n_{\mathrm{exc}}(t=0)=0$ in our case.

D. Numerical details

The presented computation results were obtained for a bulk Si sample. We employed the primitive cell of Si composed of two atoms with an experimental lattice constant, $a_0=5.431$ Å. Non-orthogonal periodic boundary conditions in all directions were used to describe the bulk crystal. Calculations of the ground state Si were performed using a real-space discretization (with grid spacing of 0.227 Å) and converged using the local density approximation (LDA) for the exchange-correlation

functional. Several TDDFT calculations were performed using a more accurate but computationally demanding TB09 meta-generalized gradient approximation for the functional.[7] Assessment of the validity of the LDA and TB09 functionals to describe the transient properties of Si is provided in Refs. [8–13]. All calculations were carried out using the open source code Octopus.[14–16] The modeling of induced fields was disabled. The atomic potential of Si is modeled using a norm-conserving pseudopotential.[17] The **k**-grid was refined until reaching a constant quantity of excited electrons. The convergence was reached with using a $24\times24\times24$ grid in the **k**-space. The integration of the KS equation was performed using the enforced time-reversal symmetry (ETRS) algorithm.[18] The time step was reduced until convergence of the excited electron density below 1% variation achieved with a time step of 6.8 attoseconds for both functionals. Note that, upon using the TB09 functional, the temporal integration was performed based on predictor-corrector method.[13] The TB09-based TDDFT results do not considerably differ from those obtained based on the LDA potential. However, further investigations are needed in this direction.

E. Introducing laser pulses with a top-hat temporal profile

The electric field of the laser pulse is introduced in the KS equation using the dipolar approximation.[4] As a consequence, the time-dependent laser field is homogeneous inside the simulation cell. The vector potential $\boldsymbol{A}(t)$ is linked with the electric field $\boldsymbol{E}(t)$ via

$$\boldsymbol{A}(t) = -c\int_{-\infty}^{t} \boldsymbol{E}(t')\,dt'. \tag{4}$$

If to approximate this integral using the slowly varying envelope approximation, the following relation can be obtained $\boldsymbol{A}(t) \sim ic\boldsymbol{E}(t)/\omega$.

We are interested in the excitation rate of the electrons transferred from the valence bands to the conduction bands. In order to provide this value on a similar basis as in the Keldysh theory where the ionization rate is averaged over laser cycles in a constant-amplitude field,[19] we introduce a "softened" top-hat (STH) laser pulse of a duration τ_p. The main part of STH pulse represents a plateau of the duration τ_p with rising and decay phases, both of the duration of τ_r, which are short compared with τ_p. The pulse is expressed as:

$$\boldsymbol{E}(t) = \boldsymbol{E}_0\cos(\omega t+\phi)\times \tag{5}$$

$$\times\begin{cases}\sin^2\left[\frac{\pi\left(t+\tau_p/2+\tau_r\right)}{2\tau_r}\right], & -\frac{\tau_p}{2}-\tau_r\le t\le-\frac{\tau_p}{2}\\ \sin^2\left[\frac{\pi\left(t-\tau_p/2\right)}{2\tau_r}\right], & \frac{\tau_p}{2}\le t\le\frac{\tau_p}{2}+\tau_r\\ 1, & |t|<\frac{\tau_p}{2}\\ 0 & |t|\ge\frac{\tau_p}{2}+\tau_r.\end{cases} \tag{6}$$

The laser frequency is given by $\omega = 2\pi c/\lambda$ and ϕ is the carrier envelope phase (CEP), which was set to 0.

The rising time τ_r for the STH pulses is used here to avoid a temporal discontinuity in the field amplitude when the laser pulse starts and terminates. The τ_r value was optimized to obtain the minimum final excited electron density. This optimum was reached for $\tau_r = 4\pi/\omega$.

II. DETAILS OF THE ANALYTICAL MODELS

A. Keldysh-Gruzdev excitation model for crystals

To calculate the number of excited electrons, several theories of electron excitation for solids were proposed[20]. Gulley *et al.* summarized the Keldysh theory without amending modifications,[21–24] whereas corrections were proposed by Gruzdev *et al.*,[25–28] to account for spin degeneracy. More recently, McDonald *et al.*[29,30] have used a model based on semiconductor Bloch equations[31] to further study the effect of band dispersion in electron excitation where not only the envelope of the pulse but also the phase of the laser pulse can be accounted for.

In this Section the analytical model is detailed, which was used to calculate the $w_{\mathrm{PI}}^{\mathrm{KG}}$ values which are shown in Figs. 2–3 of the main manuscript. The Kane band structure, which is applicable for narrow band gap materials,[27] is considered in this model. In the general form, the nonlinear photoionization rate $w_{\mathrm{PI}}(I)$ in a constant-amplitude field is expressed as

$$\frac{\partial n_{\mathrm{exc}}(I)}{\partial t} = w_{\mathrm{PI}}(I). \tag{7}$$

According to the Keldysh-Gruzdev excitation model, the photoionization rates are expressed as

$$w_{\mathrm{PI}}^{\mathrm{KG}}(I) = 2\times\frac{2\omega}{9\pi}\left(\frac{m^*\omega}{\hbar F_1}\right)^{\frac{3}{2}}F_0\times \tag{8}$$
$$\exp\left(-\pi\left[\frac{U_{\mathrm{eff}}}{\hbar\omega}+1\right]\times\frac{\hat{K}(F_1)-\hat{E}(F_1)}{\hat{E}(F_2)}\right)$$

with

$$F_0 = \sqrt{\frac{\pi}{2\hat{K}(F_2)}}\sum_{n=0}^{\infty}\left[\exp\left(-\frac{\pi n\left[\hat{K}(F_1)-\hat{E}(F_1)\right]}{\hat{E}(F_2)}\right)\times\right. \tag{9}$$
$$\left.\times G\left(\pi\sqrt{\frac{\left[\frac{U_{\mathrm{eff}}}{\hbar\omega}+1\right]-\frac{U_{\mathrm{eff}}}{\hbar\omega}+n}{2\times\hat{K}(F_2)\times\hat{E}(F_2)}}\right)\right].$$

Here $m^* = 0.2226m_e$ is the electron effective mass with m_e to be the electron mass in vacuum;[32] $n = \lceil U_{\mathrm{eff}}/\hbar\omega\rceil$ is the number of photons per electron for overcoming the effective potential barrier. Expression (9) employs the Dawson integral $G(z) = \int_0^z dy\, e^{y^2-z^2}$, which is calculated numerically. $\hat{K}(x)$ and $\hat{E}(x)$ are the complete elliptic integrals of the first and second kind respectively, which

have the forms $\hat{K}(x) = \int_0^{\pi/2} \left[1 - x^2 \sin^2\theta\right]^{-1/2} d\theta$ and $\hat{E}(x) = \int_0^{\pi/2} \sqrt{1 - x^2 \sin^2\theta}\, d\theta$. The effective ionization potential U_{eff} accounts for the energy shift induced by the Stark effect that can be written as $U_{\text{eff}} = \frac{2E_g}{\pi F_1}\hat{E}(F_2)$. F_1 and F_2 are the functions of the adiabaticity parameter γ: $F_1 = \gamma/\sqrt{1+\gamma^2}$, $F_2 = F_1/\gamma$. The γ value is given by

$$\gamma = \frac{\omega\sqrt{m^* E_g}}{eE_{\text{peak}}} = \frac{\omega\sqrt{m^* E_g}}{e\sqrt{\frac{2I_{\text{peak}}}{c\varepsilon_0}}}. \tag{10}$$

It characterizes irradiation regimes via the peak intensity I_{peak} or the electric field amplitude E_{peak}. When $\gamma \ll 1$, the electron excitation from the valence band to the conduction band occurs via tunneling ionization whereas $\gamma \gg 1$ corresponds to multiphoton ionization. For $\gamma \ll 1$, the Keldysh model for crystals describes the tunneling mechanism of photoionization in the form

$$w_{\text{PI}}^{\text{tun}} = \frac{2}{9\pi^2}\frac{E_g}{\hbar}\left(\frac{m^* E_g}{\hbar^2}\right)^{3/2}\left(\frac{e\hbar E_{\text{peak}}}{(m^*)^{1/2}E_g^{3/2}}\right)^{5/2} \times \exp\left[-\frac{\pi}{2}\frac{(m^*)^{1/2}E_g^{3/2}}{e\hbar E_{\text{peak}}}\left(1 - \frac{1}{8}\frac{m^*\omega^2 E_g}{e^2 E_{\text{peak}}^2}\right)\right], \tag{11}$$

where E_g is the bare band gap energy.[27] Note that this formula is not applicable at low fields where ionization is governed by the multiphoton mechanism.[33]

B. Keldysh ionization model for atomic gases: analytical and numerical integration

In this section, the formulas of the Keldysh theory for ionization of an atomic gas are provided. We have employed the analytical atomic Keldysh model given by Eqs. (16)-(18) from Ref. [19] to compare this theory with both TDDFT and the Keldysh theory for excitation of band gap solids (see Fig. 2 of the main manuscript):

$$w_{\text{PI}}^{\text{at}} = \rho \times \omega\sqrt{\frac{2E_g}{\hbar\omega}}\left(\frac{\gamma}{\sqrt{1+\gamma^2}}\right)^{3/2} S\left(\gamma, \frac{U_{\text{eff}}}{\hbar\omega}\right) \times \exp\left[-\frac{2U_{\text{eff}}}{\hbar\omega}\frac{\operatorname{arcsinh}(\gamma) - \gamma\sqrt{1+\gamma^2}}{1+2\gamma^2}\right], \tag{12}$$

where

$$S(\gamma, x) = \sum_{n=0}^{\infty} \exp\left[(-2\lceil x+1\rceil - x + n)\times\left(\operatorname{arcsinh}(\gamma) - \frac{\gamma}{\sqrt{1+\gamma^2}}\right)\right] \times G\left(\frac{2\gamma}{\sqrt{1+\gamma^2}}\sqrt{\lceil x+1\rceil - x + n}\right).$$

The Dawson integral $G(z)$ is given in Section II A.

Numerical integration. We use an estimative adaptation of material photoionization based on the Keldysh theory for atoms.[19] For this aim, we consider a virtual hydrogen-like atom with the energy of its ground state equal to the material band gap, $E_g^{\Gamma} = 2.56$ eV.[12] The electron of the atom has mass m^*, which is taken to be the same as in both the Keldysh theory for band gap solids (Eqs. (7)-(9)) and the TDDFT simulations. This gives formulas for the ionization probability of atoms analogous to Ref. [19]. Note that the ionization rate (Eq. (12)) is multiplied by the atomic density of the solid ρ (silicon in our case) to express the rate in $\text{m}^{-3}\text{s}^{-1}$.

When solving Eq. (12), we calculated the integrals numerically instead of using the saddle-point method. The integrals have the following form

$$P = \frac{\omega}{2\pi}\int_0^{2\pi/\omega} dt\, F(t)\, e^{i\eta(t)}.$$

To calculate the integrals, a fine temporal grid $t_k = k \times \tau$ ($k = 0, ..., N_t$; $\tau = \frac{2\pi}{N_t\omega}$) was used. Within the time segments $t_{k-1} < t < t_{k+1}$, the function F is approximated by the polynomial

$$F(t) = F_k + \frac{F_{k+1} - F_{k-1}}{2\tau}(t - t_k) + \frac{F_{k+1} - 2F_k + F_{k-1}}{2\tau^2}(t - t_k)^2$$

For η, the linear expansion is used, $\eta = \eta_k + v_k(t - t_k)$ with $v_k = \frac{\eta_{k+1} - \eta_{k-1}}{2\tau}$. Consequently, we have

$$P \simeq \frac{\omega}{2\pi}\sum_{k=1}^{N_t - 1} e^{i\eta_k}\int_{-\tau}^{\tau} d\sigma e^{iv_k\sigma}\left[F_k + \frac{F_{k+1} - F_{k-1}}{2\tau}\sigma + \frac{F_{k+1} - 2F_k + F_{k-1}}{2\tau^2}\sigma^2\right].$$

Such calculations of integrals are time-efficient and sufficiently precise, provided that the time step τ is much smaller than the laser cycle.

III. THE TDDFT RESULTS FOR DIFFERENT WAVELENGTHS; FITTING OF THE KG MODEL

According to our TDDFT simulations, the first principles approach yields photoionization rates, which are at least an order of magnitude higher as compared to the Keldysh theory for solids. This has systematically been studied at different laser wavelengths, see Figs. 1–3. We remind that, in our study, the fields induced by the movement of charges in the time-propagation of KS orbitals were disregarded (Eq. (1)). Under this assumption, the laser pulse inside a bulk material is compressed with the intensity multiplied by the material refractive index and it should be the same both in TDDFT simulations and in the Keldysh formulas. However, the TDDFT approach includes several important factors, which are absent in

the Keldysh theory and thus can be responsible for the observed discrepancy.

One of the most important factors is the realistic bandgap structure introduced in TDDFT, which is dynamically varying upon electron excitation into the conduction bands with corresponding distortion of interatomic potential. As a result, the electron wave functions are subjected to the action of the field of the laser wave superimposed with the dynamic interatomic field. One can anticipate that the local field acting on the electronic component of the crystal is enhanced similarly to predictions of Gaier *et al.*[34] while not necessarily in a fluctuation manner. Another factor, also connected with the dynamic band structure, is the so-called laser dressing of the electronic states or, by other words, appearance of transient quasi-states usually referred as the Wannier-Stark ladder.[35] We can also mention the Abraham-Minkowski problem[36] connected with the momentum of photons inside material, which still calls for investigations. Although this goes beyond the scope of the present study, a particular attention on the role of induced fields in the conservation of the momentum at interfaces is envisioned.[6]

Figures 2(b) and 3(b) show that the KG model underestimates the results of the TDDFT simulations where the band structure is more realistic and laser dressing is naturally addressed. Interesting is to find a factor ζ of "laser field amplification", $E \to \zeta E$, at which the KG model would fit the TDDFT results. We have performed this procedure for different wavelengths and the results are presented in Figs. 1(b), 2(c), and 3(c) respectively for 3200, 1600, and 800 nm for both the KG model and its tunneling limit. By choosing the ζ value, it was surprisingly found that the accurate enough fits were achieved at $\zeta = \sqrt{n(\lambda)}$ where n is the refractive index at the corresponding wavelength λ. It is not clear yet if it is a pure coincidence or it hides a physical cause. The TDDFT simulations for other materials and their comparison with the corresponding Keldysh solutions can help to clarify this puzzling question that is now under development. Also interesting is that for all studied wavelengths the atomic Keldysh theory applied for our virtual atom agrees reasonably with the TDDFT simulation results at low intensities (in the multiphoton regime, see Figs. 1–3).

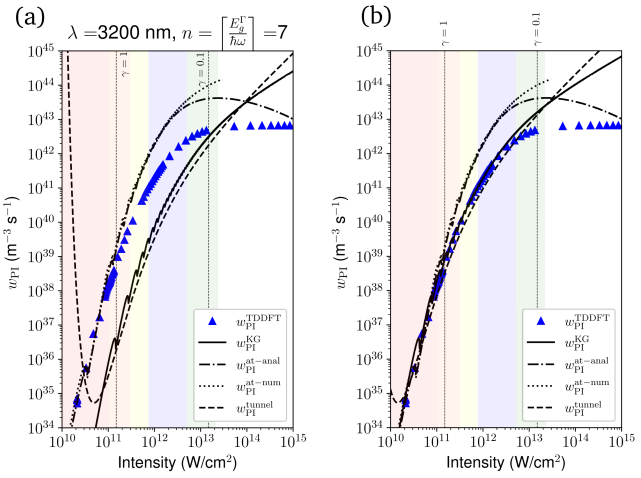

Figure 1. (a) Comparison of photoionization rates as a function of laser intensity inside silicon crystal obtained in the TDDFT simulations, $w_{\rm PI}^{\rm TDDFT}$, after the laser pulse termination (τ_p = 30 fs, λ = 3200 nm) with the analytical theories: the KG ionization rate $w_{\rm PI}^{\rm KG}$, the tunneling ionization rate, $w_{\rm PI}^{\rm tunnel}$, and the Keldysh photoionization rates for a virtual atom (Eq. (12), see text) obtained using the saddle-point method, $w_{\rm PI}^{\rm at\text{-}anal}$, and with numerically calculated integrals, $w_{\rm PI}^{\rm at\text{-}num}$. (b) The same as in (a) but with fitting the KG and tunneling rates to the TDDFT results using normalization of the laser field in the KG formulas using the factor $\zeta = \sqrt{n(\lambda)}$ (see text).

IV. LASER DRESSING, EFFECT OF RABI OSCILLATIONS AND THE ROLE OF BESSEL FUNCTIONS IN STRONG FIELD EXCITATION

During laser action, response of a bandgap material to irradiation can be described by shifting the energy levels of the band structure as compared with the ground state structure.[37,38] This shift is known as laser dressing and it originates from the coupling of laser light to the electrons, which lasts the time of the laser illumination. As a result of the light-induced periodic electron motion, the dressed band structure does not represent anymore purely electronic states. Instead, the dressed energy levels are considered as quasi-particles named polaritons. This vision is not new and it was already employed in a number of formalisms, e.g., already in the Keldysh theory,[19] in atomic physics[39] and in the non-equilibrium solid state physics.[40,41] Laser dressing may lead to ultrafast transient metallization,[42,43] a phenomenon that has enabled the development of novel applications in ultrafast optoelectronics.[44]

As stated in Ref. [42], a qualitative description of the laser dressing effect is possible from the knowledge of the electronic ground state. We underline that the approach employed here is based on a simplified model Hamiltonian. In particular, the importance of the term scaling in A^2 in the employed Hamiltonian, which is disregarded in our approach, was investigated in a series of recent publications.[41,45] Also the dipolar matrix elements should be affected by intense laser fields, a phenomenon that is not described in the simplified method we have employed to prepare Fig. 1 of the main manuscript, which therefore should be considered as a contextual illustration.

In Fig. 3(a,b) of the main manuscript, the minima of the excitation rates $w_{\rm PI}^{KG}(\hbar\omega)$ provided by the KG theory are outlined by grey lines. These reductions of $w_{\rm PI}(\hbar\omega)$ are pronounced in the Keldysh theory and are also visible in the TDDFT simulation results, though mildly.

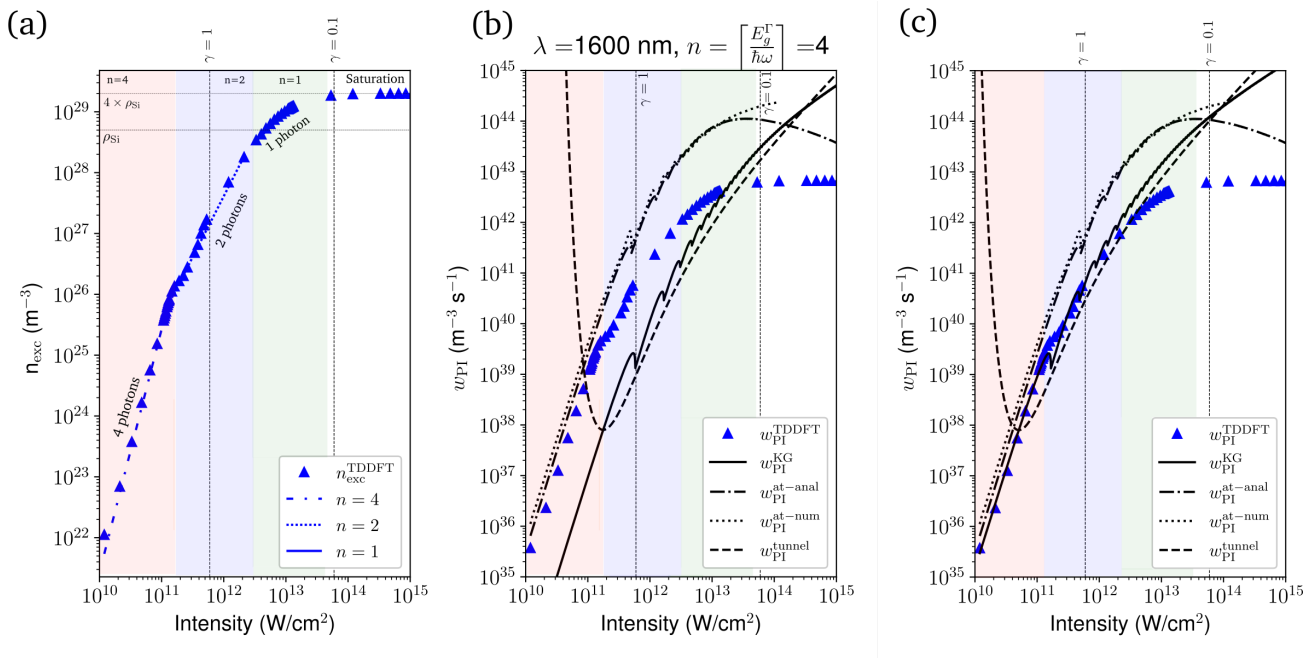

Figure 2. The data for 1600 nm wavelength. (a) Electron density in the conduction bands after laser pulse termination (τ_p = 30 fs). Lines fitting the computed σ_n values are indicated. (b) and (c) are the same as in Figs. 1(a) and 1(b) respectively for another wavelength.

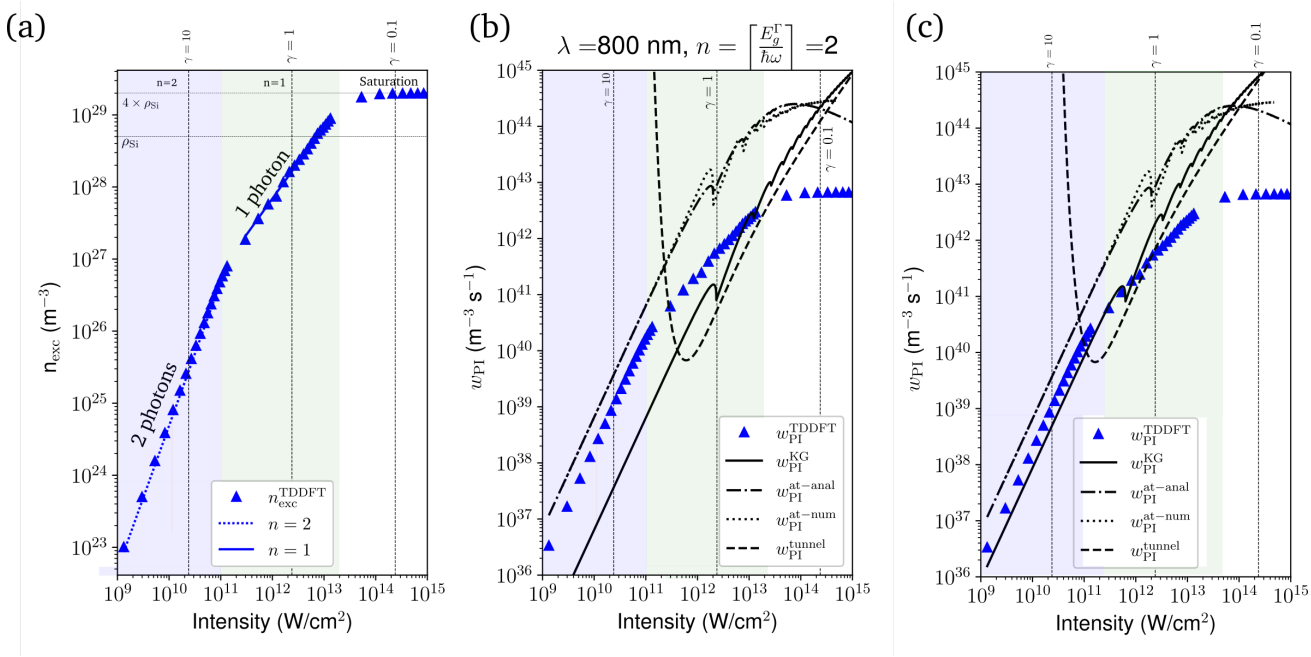

Figure 3. The same as in Fig. 2 for 800 nm wavelength.

In literature, the origin of such reductions of the amplitude probability $w_{\mathrm{PI}}(\hbar\omega)$ was attributed to the suppression of tunneling[46–48] (equivalently, these are described in the real-space as Wannier-Stark localization[35,49,50]). The tunneling drop interpretation can be illustrated by an analytical solution constructed from a simplified Hamiltonian model describing the effect of the laser field on the conduction electronic subsystem.[46–48] Using a rigid band viewpoint, a series of the Bessel functions of n-th order appear in the corresponding analytical solution as a multiplicative term for each replication order n.[46–48] Since the Bessel function is inside the sum of possible wave-

functions, an eventual suppression of interband transitions depends on the number of available electronic levels.

In a two-band description as in the Keldysh theory, suppression of the transition from one band to the other may take place when the Rabi frequency is twice the laser photon frequency[46–48]

$$J_n\left(\frac{2\Omega_{\text{Rabi}}}{\omega_{\text{laser}}}\right) = 0. \tag{13}$$

However, when several electronic energy levels are available, a simultaneous suppression of all possible transitions (a transition is denoted by its dipolar matrix element $d_{i\to j}$) may not be feasible. Assuming that the total transition probability can be reasonably described by a series of Bessel functions in the physical reality, the *Le Bourget* theorem[51] suggests that *only one* transition could be possibly disabled for a given set of laser parameters (electric field of the wave, wavelength). This mathematical argument provides a physical explanation for rather smooth reduction of total transition probability w_{PI} observed in multiband description such as TDDFT (Fig. 3(b)) while a two-band description such as the Keldysh model reveals a clear suppression of transitions at given resonant frequencies [Fig. 3(a)]. Then, since the Rabi frequency is proportional to $\Omega_{\text{Rabi}} \propto E \cdot d_{i,j}$ (E is the field amplitude), Eq. (13) can be rewritten as

$$J_n\left(\frac{2E \cdot d_{i,j}}{\hbar\omega^2}\right) = 0 \tag{14}$$

where $J_n(x)$ denotes the Bessel function of n-th order. The dipolar transition matrix elements $d_{i,j} = \langle\psi_i|\hat{r}|\psi_j\rangle$ were obtained from the DFT computation. Figure 4 depicts the value of the dipolar matrix elements for Si in atomic units. The elements indexed from 0 to 3 correspond to the valence band states, the rest correspond to the conduction states. Since the description of the Hamiltonian is hermitian, the matrix elements are symmetric above and below the matrix diagonal, evidencing the equivalent transition probabilities for excitation and recombination in the linear regime. Knowing the nodes of the Bessel functions of n-th order, an illustrative mapping of the transition to be selectively disabled can be provided (Fig. 5).

V. SIMPLIFIED MODEL OF LASER ENERGY ABSORPTION

Energy absorbed by electrons. The energy $\xi_{\text{el}}^{\text{TDDFT}}(t)$ absorbed by the electrons is calculated as the difference between time-dependent electron energy $e_{\text{el}}^{\text{TDDFT}}(t)$ and the ground state energy $\xi_{\text{el}}^{\text{TDDFT}}(t) = e_{\text{el}}^{\text{TDDFT}}(t) - e_{\text{el}}^{\text{TDDFT}}(t=0)$. To calculate the total energy of electrons $e_{\text{el}}^{\text{TDDFT}}(t)$, the formula given in the Appendix H of Ref. [52] was used (it is also given in Chapter 5 of Ref. [4]).

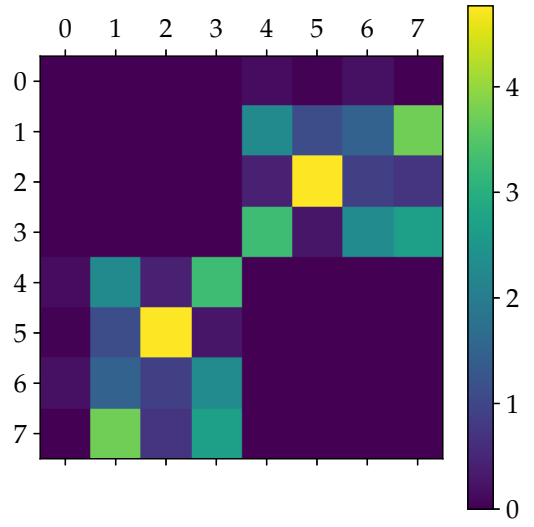

Figure 4. The values of the dipolar matrix elements $\log_{10} d_{i,j}$ obtained from the ground state of Si crystal (space group 227) via calculations using the LDA functional.

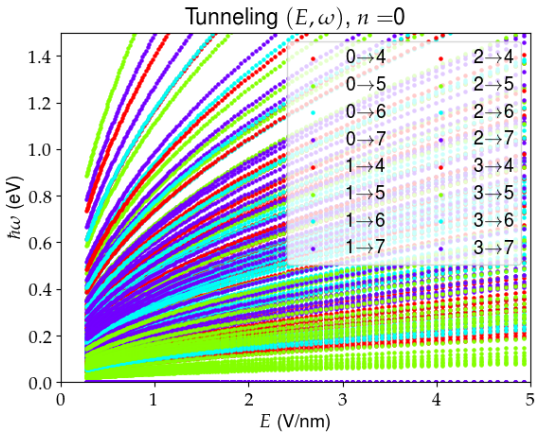

Figure 5. Selective transition removal as a function of the laser parameters $(E, \hbar\omega)$ [E: field amplitude, $\hbar\omega$ is the photon energy] for the transitions of zero-th order ($n = 0$).

Electron excess energy. The energy density $de(\boldsymbol{r}, t)$ introduced into the sample by the laser at each time interval dt can be expressed using the total current density $\boldsymbol{j}(\boldsymbol{r}, t)$ and the laser electric field $\boldsymbol{E}(\boldsymbol{r}, t)$ as

$$\frac{de(\boldsymbol{r}, t)}{dt} = \underbrace{\boldsymbol{j}(\boldsymbol{r}, t) \cdot \boldsymbol{E}(\boldsymbol{r}, t)}_{\text{total absorption (inter+intra)}} . \tag{15}$$

Usually the total current is separated to contributions from the polarization (originating from interband transitions) and the free carrier current $\boldsymbol{j}_{\text{free}}(t)$ related to

intraband processes. The dynamics of the absorbed energy density $e(\boldsymbol{r},t)$ can be described as

$$\frac{de(\boldsymbol{r},t)}{dt} \simeq \underbrace{n\hbar\omega \times w_{\mathrm{PI}}(\boldsymbol{r},t)}_{\text{interband absorption}} + \underbrace{\boldsymbol{j}_{\mathrm{free}}(\boldsymbol{r},t)\cdot\boldsymbol{E}(\boldsymbol{r},t)}_{\text{intraband absorption}}, \tag{16}$$

where $w_{\mathrm{PI}}(\boldsymbol{r},t)$ is the instantaneous photoionization rate and $n = \left\lceil \frac{E_{\mathrm{gap}}}{\hbar\omega} \right\rceil$ is the number of photons that are required to overcome the bare band gap energy E_{gap} using the electric field of the laser wave at frequency ω. In order to compare with the total energy, calculated by solving the KS equation (Eq. 1), we integrate Eq. (16) over time in a volume V as

$$\xi_{\mathrm{el}}(t) = \int_V d^3r\, e(\boldsymbol{r},t) \simeq \int_V d^3r\, n\hbar\omega \times n_{\mathrm{exc}}(\boldsymbol{r},t) + \int_V d^3r \int_0^t dt'\, \boldsymbol{j}_{\mathrm{free}}(\boldsymbol{r},t')\cdot\boldsymbol{E}(\boldsymbol{r},t'). \tag{17}$$

The density n_{exc} is calculated by Eq. (2). Using the dipolar approximation for the external field, we obtain the energy ξ_{el} received by electrons from the laser field, which is defined as

$$\xi_{\mathrm{el}}(t) = \int_V d^3r\, n\hbar\omega \times n_{\mathrm{exc}}(\boldsymbol{r},t) + \int_0^t dt'\, \boldsymbol{J}_{\mathrm{free}}(t')\cdot\boldsymbol{E}(t'). \tag{18}$$

Time-dependent description of the free-carrier absorption The energy transferred from the laser light to the electrons via intraband absorption can be computed from the excited electron density $n_{\mathrm{exc}}(t)$ and the conduction band electron current $\boldsymbol{J}_{\mathrm{free}}(t)$ by using of the generalized Ohm law, expressed by

$$\boldsymbol{J}_{\mathrm{free}}(t) = \int dt' \sigma_{\mathrm{free}}(t,t')\,\boldsymbol{E}(t').$$

The contribution of the free electron currents can be described using a time-dependent conductivity $\sigma_{\mathrm{free}}(\omega;t) = -i\omega\varepsilon_0\left[\varepsilon_{\mathrm{Drude}}(\omega;t) - 1\right]$, where the dielectric permittivity $\varepsilon_{\mathrm{Drude}}(t,\omega)$ is given by the Drude model for solids[53]

$$\varepsilon_{\mathrm{Drude}}\left[n_{\mathrm{exc}}(t)\right](\omega) = 1 - \frac{e^2}{m_e m_{\mathrm{eff}}\varepsilon_0\omega^2} \times \frac{n_{\mathrm{exc}}(t)}{1 + i\frac{\nu}{\omega}}. \tag{19}$$

The electron collision (or damping) time $\tau_D = \nu^{-1}$ is usually considered to be from one to several femtoseconds. In this work, the effective electron mass is taken as given by the DFT,[32] $m_{\mathrm{eff}} = 0.2226$. The collision time $\tau_D = 6$ fs was adjusted to obtain the best fit to the TDDFT simulation results (see Fig. 4 of the main manuscript).

Modeling the excess energy. Finally, with the above assumptions, we derive from Eq. (18) the balance equation for the excess electron energy ξ_{Drude} based on the Drude model, which reads as

$$\frac{\partial\xi_{\mathrm{Drude}}}{\partial t} = V\left[n\hbar\omega w_{\mathrm{PI}}(t) + 2\pi\varepsilon_0\int d\omega\,\omega\mathrm{Im}\left[\varepsilon(\omega)\right]\boldsymbol{E}(\omega)^2\right]. \tag{20}$$

In the case of a quasi-continuous wave of frequency centered at ω_0, one has $\boldsymbol{E}(\omega) \to \delta(\omega \pm \omega_0)\,\boldsymbol{E}(\omega)$ that yields

$$\frac{\partial\xi_{\mathrm{Drude}}}{\partial t} = V\left[n\hbar\omega w_{\mathrm{PI}}(t) + \varepsilon_0\omega_0\mathrm{Im}\left[\varepsilon(\omega_0)\right]\boldsymbol{E}(\omega_0)^2\right].$$

To calculate the absorbed electron energy at a time moment t in a volume V, we integrate the above expression over time from $t = 0$ to t that gives

$$\begin{aligned}\xi_{\mathrm{Drude}}(t) = \\ V\int_0^t dt'\left[n\hbar\omega w_{\mathrm{PI}}(t') + \varepsilon_0\omega_0\mathrm{Im}\left\{\varepsilon\left[n_{\mathrm{exc}}(t')\right](\omega_0)\right\}\boldsymbol{E}(\omega_0)^2\right] \\ = Vn\hbar\omega n_{\mathrm{exc}}(t) + \\ + V\int_0^t dt'\varepsilon_0\omega_0\mathrm{Im}\left\{\varepsilon\left[n_{\mathrm{exc}}(t')\right](\omega_0)\right\}\boldsymbol{E}(\omega_0)^2.\end{aligned} \tag{21}$$

The later expression depends on the excited electron density $n_{\mathrm{exc}}(t)$ and on three free parameters, namely the electron collision frequency ν, the electron effective mass m_{eff}, and the band gap energy E_{gap}. We used Eq. (21) to compare it with the electron excess energy $\xi_{\mathrm{el}}^{\mathrm{TDDFT}}$ obtained in our TDDFT simulations.

VI. EXCITATION PROBABILITIES AS A FUNCTION OF LASER PARAMETERS

From the calculated dependences $n_{\mathrm{exc}}^{\mathrm{TDDFT}}(I_{\mathrm{peak}})$, the effective multiphoton rates σ_n associated with $n-$photon transitions can be extrapolated using the multiphoton approximation expressed by

$$\frac{\partial n_{\mathrm{exc}}^{\mathrm{TDDFT}}}{\partial t} = \sigma_n\frac{I^n}{n\hbar\omega}. \tag{22}$$

We remind that the LDA functional can underestimate the bandgap energy of crystals, which is usually smaller as compared to more sophisticated modeling approaches for band structure calculations.[12] Therefore, we have to note that here the effective multiphoton excitation rates σ_n for silicon were calculated for the direct bandgap energy, which is somewhat smaller than the experimentally measured value. Using Eq. (22), one can fit the TDDFT results from Figs. 1(a), 2(b), and 3(b), thus deriving the σ_n values. The data are summarised in Table I for the intensities below the saturation regimes. Where possible, we provide comparison of our data with the multiphoton excitation rates available in the literature. As one can see, a reasonable agreement is achieved although in experimental studies pure multiphoton excitation can be

Method	Wavelength	τ_p	Band gap	Intensity range (W/cm^2)	Eff. transition probability	Ref.
Theory (TD-LDA)	3200 nm	30 fs	2.56 eV (d)	$(2.1-9.9)\times10^{10}$	$\sigma_5\,(\mathrm{m^7W^{-4}}) = 4.84\times10^{-56}$	This work
				$(1.0-2.6)\times10^{11}$	$\sigma_4\,(\mathrm{m^5W^{-3}}) = 3.05\times10^{-41}$	This work
				$(2.6-5.3)\times10^{11}$	$\sigma_3\,(\mathrm{m^3W^{-2}}) = 5.25\times10^{-26}$	This work
				$(0.53-3.4)\times10^{12}$	$\sigma_2\,(\mathrm{mW^{-1}}) = 2\times10^{-10}$	This work
				$(0.34-1.0)\times10^{13}$	$\sigma_1\,(\mathrm{m^{-1}}) = 2.93\times10^{6}$	This work
		20 fs	2.56 eV (d)	$(0.2-1.0)\times10^{11}$	$\sigma_5\,(\mathrm{m^7W^{-4}}) = 5.38\times10^{-56}$	This work
				$(1.0-2.6)\times10^{11}$	$\sigma_4\,(\mathrm{m^5W^{-3}}) = 3.42\times10^{-41}$	This work
				$(0.26-0.64)\times10^{12}$	$\sigma_3\,(\mathrm{m^3W^{-2}}) = 6.12\times10^{-26}$	This work
				$(0.6-3.4)\times10^{12}$	$\sigma_2\,(\mathrm{mW^{-1}}) = 2.52\times10^{-10}$	This work
				$(0.34-1)\times10^{13}$	$\sigma_1\,(\mathrm{m^{-1}}) = 3.94\times10^{6}$	This work
		10 fs	2.56 eV (d)	$(0.21-1.07)\times10^{11}$	$\sigma_5\,(\mathrm{m^7W^{-4}}) = 6.52\times10^{-56}$	This work
				$(1.07-2.9)\times10^{11}$	$\sigma_4\,(\mathrm{m^5W^{-3}}) = 4.37\times10^{-41}$	This work
				$(0.29-0.82)\times10^{12}$	$\sigma_3\,(\mathrm{m^3W^{-2}}) = 7.27\times10^{-26}$	This work
				$(0.82-3.4)\times10^{12}$	$\sigma_2\,(\mathrm{mW^{-1}}) = 3.92\times10^{-10}$	This work
				$(0.34-1)\times10^{13}$	$\sigma_1\,(\mathrm{m^{-1}}) = 6.38\times10^{6}$	This work
Exp.		200 fs			$\sigma_3\,(\mathrm{m^3W^{-2}}) = 0.5\times10^{-26}$	Pearl *et al.*[54]
Theory (TD-LDA)	1600 nm	30 fs	2.56 eV (d)	$(0.11-1.6)\times10^{11}$	$\sigma_4\,(\mathrm{m^5W^{-3}}) = 4.41\times10^{-40}$	This work
				$(0.14-3.2)\times10^{12}$	$\sigma_2\,(\mathrm{mW^{-1}}) = 3.39\times10^{-10}$	This work
				$(0.32-1.6)\times10^{13}$	$\sigma_1\,(\mathrm{m^{-1}}) = 4.14\times10^{6}$	This work
		20 fs	2.56 eV (d)	$(0.11-1.6)\times10^{11}$	$\sigma_4\,(\mathrm{m^5W^{-3}}) = 4.62\times10^{-40}$	This work
				$(0.16-3.2)\times10^{12}$	$\sigma_2\,(\mathrm{mW^{-1}}) = 4.43\times10^{-10}$	This work
				$(0.32-1.3)\times10^{13}$	$\sigma_1\,(\mathrm{m^{-1}}) = 5.48\times10^{6}$	This work
Exp.		200 fs	1.12 eV (i)		$\sigma_2\,(\mathrm{mW^{-1}}) = 1.9\times10^{-11}$	Bristow *et al.*[55]
Theory (TD-LDA)	800 nm	30 fs	2.56 eV (d)	$(0.12-14)\times10^{10}$	$\sigma_2\,(\mathrm{mW^{-1}}) = 8.05\times10^{-9}$	This work
				$(0.01-1.4)\times10^{13}$	$\sigma_1\,(\mathrm{m^{-1}}) = 5.72\times10^{6}$	This work
		20 fs	2.56 eV (d)	$(0.12-14)\times10^{10}$	$\sigma_2\,(\mathrm{mW^{-1}}) = 8.99\times10^{-9}$	This work
				$(0.14-14)\times10^{12}$	$\sigma_1\,(\mathrm{m^{-1}}) = 8.02\times10^{6}$	This work
		10 fs	2.56 eV (d)	$(0.12-14)\times10^{10}$	$\sigma_2\,(\mathrm{mW^{-1}}) = 1.07\times10^{-8}$	This work
				$(0.14-14)\times10^{12}$	$\sigma_1\,(\mathrm{m^{-1}}) = 1.45\times10^{7}$	This work
Exp.	550 nm to 620 nm	90 fs	1.12 eV (i)		$9\times10^{-11} < \sigma_2\,(\mathrm{mW^{-1}}) < 36\times10^{-11}$	Reitze *et al.*[56]
Exp.	800 nm	200 fs	1.12 eV (i)		$\sigma_2\,(\mathrm{mW^{-1}}) = 1.9\times10^{-11}$	Bristow *et al.*[55]
Exp.	800 nm	-	1.12 eV (i)		$\sigma_2\,(\mathrm{mW^{-1}}) = 6.8\times10^{-11}$	Sjodin *et al.*[57]
Exp.	1060 nm		1.12 eV (i)		$\sigma_2\,(\mathrm{mW^{-1}}) = 1.5\times10^{-11}$	T.F. Boggess[58]
Theory (TD-LDA)	483 nm	20 fs	2.56 eV (d)	$(0.01-100)\times10^{11}$	$\sigma_1\,(\mathrm{m^{-1}}) = 1.09\times10^{7}$	This work
Theory (TD-TB09)	407.58 nm	20 fs	3.04 eV (d)	$(0.01-140)\times10^{11}$	$\sigma_1\,(\mathrm{m^{-1}}) = 1.074\times10^{7}$	This work
Exp.	483 nm	-	1.12 eV (i)		$\sigma_1\,(\mathrm{m^{-1}}) = 2.16\times10^{6}$	E. D. Palik[59]
Exp.	407.58 nm	-	1.12 eV (i)		$\sigma_1\,(\mathrm{m^{-1}}) = 0.964\times10^{7}$	E. D. Palik[59]

Table I. Multiphoton excitation rates (σ_1, ..., σ_5) derived from the results of the first-principles simulations for the corresponding intensity ranges. The results obtained with LDA and TB09 functionals are reported. Note that the adjustments of effective multiphoton coefficients were performed in regimes where tunneling and saturation effects may play a role. Available experimental data are also reported.

masked by other processes involved at longer pulse durations such as collisional ionization and phonon-assisted indirect transitions.

We notice that for 800 nm wavelength, the value of σ_2 obtained using first-principle simulations somewhat decreases when increasing the laser pulse duration and the same is observed for other wavelengths and other σ_n. This may originate from the dynamic behavior of the excitation. Once states at the bottom of the conduction bands are populated, the excitation probability decreases rapidly, an effect known as the Burstein-Moss effect.[60] Although the multiphoton ionization rates σ_2 obtained in the first-principles calculations show a dependence on pulse duration τ_p, the σ_n values mostly remain within

the same order of magnitude. Also we have calculated the single- and two-photon absorption rates σ_1 and σ_2 using the LDA and TB09 functionals at wavelengths of 484 nm and 407.58 nm respectively, the latter in order to adjust the laser wavelength for the resonant excitation of single-photon transition, see Table I.

In the tunneling regime where the photoionization rate obtained in the TDDFT simulations scales linearly with the peak intensity, an effective tunneling ionization rate σ_1 (using Eq. (22), $n = 1$) can be estimated as a function of pulse duration. For $\lambda = 800$ nm, $\sigma_1 = 1.447 \times 10^6$ m^{-1} at $\tau_p = 10$ fs; $\sigma_1 = 7.985 \times 10^6$ m^{-1} at $\tau_p = 20$ fs; $\sigma_1 = 5.754 \times 10^6$ m^{-1} at $\tau_p = 30$ fs (not reported in the Table).

Note that the direct comparison of the TDDFT photoionization rates with the experimental values is not straightforward since the most experimental measurements involve also indirect transitions ($\Gamma \to L$). Therefore, the comparison with experimental measurements is only qualitative here. Note also that indirect band gap transition rates can be computed using TDDFT by employing a localized electric field, as was very recently shown by Noda *et al.*[61]

The full database of pulse-averaged photoionization rates obtained by our TDDFT simulations is available at `http://www.quantumlap.eu/photo-ionization-database/`.

* derrien@fzu.cz
† bulgakova@fzu.cz

[1] E. K. U. Gross, J. F. Dobson, and M. Petersilka, in *Density Functional Theory II* (Springer, 1996) pp. 81–172.
[2] M. A. L. Marques, N. T. Maitra, F. M. S. Nogueira, E. K. U. Gross, and A. Rubio, eds., *Fundamentals of Time-Dependent Density Functional Theory*, Lecture Notes in Physics (Springer, New York, 2011).
[3] M. Ruggenthaler, N. Tancogne-Dejean, J. Flick, H. Appel, and A. Rubio, Nat. Rev. Chem. **2**, 0118 (2018).
[4] C. A. Ullrich, *Time-Dependent Density-Functional Theory: Concepts and Applications* (Oxford University Press, USA, 2012).
[5] T. Otobe, M. Yamagiwa, J.-I. Iwata, K. Yabana, T. Nakatsukasa, and G. F. Bertsch, Phys. Rev. B **77**, 165104 (2008).
[6] K. Yabana, T. Sugiyama, Y. Shinohara, T. Otobe, and G. F. Bertsch, Phys. Rev. B **85**, 045134 (2012).
[7] F. Tran and P. Blaha, Phys. Rev. Lett. **102**, 226401 (2009).
[8] E. K. U. Gross and W. Kohn, Phys. Rev. Lett. **55**, 2850 (1985).
[9] R. W. Godby, M. Schlüter, and L. J. Sham, Phys. Rev. Lett. **56**, 2415 (1986).
[10] O. Sugino and R. Car, Phys. Rev. Lett. **74**, 1823 (1995).
[11] J. M. Zuo, P. Blaha, and K. Schwarz, J. Phys.: Condens. Matter **9**, 7541 (1997).
[12] D. Waroquiers, A. Lherbier, A. Miglio, M. Stankovski, S. Poncé, M. J. T. Oliveira, M. Giantomassi, G.-M. Rignanese, and X. Gonze, Phys. Rev. B **87**, 075121 (2013).
[13] S. A. Sato, Y. Taniguchi, Y. Shinohara, and K. Yabana, J. Chem. Phys. **143**, 224116 (2015).
[14] M. A. Marques, A. Castro, G. F. Bertsch, and A. Rubio, Comput. Phys. Commun. **151**, 60 (2003).
[15] A. Castro, H. Appel, M. Oliveira, C. A. Rozzi, X. Andrade, F. Lorenzen, M. A. L. Marques, E. K. U. Gross, and A. Rubio, phys. status solidi (b) **243**, 2465 (2006).
[16] X. Andrade, J. Alberdi-Rodriguez, D. A. Strubbe, M. J. T. Oliveira, F. Nogueira, A. Castro, J. Muguerza, A. Arruabarrena, S. G. Louie, A. Aspuru-Guzik, A. Rubio, and M. A. L. Marques, J. Phys.: Condens. Matter **24**, 233202 (2012).
[17] N. Troullier and J. L. Martins, Phys. Rev. B **43**, 1993 (1991).
[18] A. Castro, M. A. L. Marques, and A. Rubio, J. Chem. Phys. **121**, 226401 (2004).
[19] L. V. Keldysh, Sov. Phys. JETP **20**, 1307 (1965).
[20] C. Mézel, A. Bourgeade, and L. Hallo, Phys. Plasmas **17**, 113504 (2010).
[21] J. R. Gulley and W. M. Dennis, Phys. Rev. A **81**, 033818 (2010).
[22] J. R. Gulley, S. W. Winkler, W. M. Dennis, C. M. Liebig, and R. Stoian, Phys. Rev. A **85**, 013808 (2012).
[23] J. R. Gulley and T. E. Lanier, Phys. Rev. B **90**, 155119 (2014).
[24] J. R. Gulley, J. Liao, and T. E. Lanier, Proc. SPIE **8972**, 89720T (2014).
[25] V. Gruzdev, Phys. Rev. B **75**, 205106 (2007).
[26] V. Gruzdev, AIP Conf. Proc. **1278**, 131 (2010).
[27] V. Gruzdev, Opt. Eng. **53**, 122515 (2014).
[28] P. Jürgens, M. Jupé, M. Gyamfi, and D. Ristau, Proc. SPIE **10014**, 100141C (2016).
[29] C. R. McDonald, G. Vampa, G. Orlando, P. B. Corkum, and T. Brabec, J. Phys. Conf. Ser. **594**, 012021 (2015).
[30] C. R. McDonald, G. Vampa, P. B. Corkum, and T. Brabec, Phys. Rev. Lett. **118**, 173601 (2017).
[31] V. Turkowski and C. A. Ullrich, Phys. Rev. B **77**, 075204 (2008).
[32] J. Laflamme Janssen, Y. Gillet, S. Poncé, A. Martin, M. Torrent, and X. Gonze, Phys. Rev. B **93**, 205147 (2016).
[33] A. Kaiser, B. Rethfeld, M. Vicanek, and G. Simon, Phys. Rev. B **61**, 11437 (2000).
[34] L. N. Gaier, M. Lein, M. I. Stockman, P. L. Knight, P. B. Corkum, M. Y. Ivanov, and G. L. Yudin, J. Phys. B: At. Mol. Opt. Phys. **37**, L57 (2004).
[35] C. Schmidt, J. Bühler, A.-C. Heinrich, J. Allerbeck, R. Podzimski, D. Berghoff, T. Meier, W. G. Schmidt, C. Reichl, W. Wegscheider, D. Brida, and A. Leitenstorfer, Nat. Commun. **9**, 2890 (2018).
[36] M. Partanen, T. Häyrynen, J. Oksanen, and J. Tulkki, Phys. Rev. A **95**, 063850 (2017).
[37] L. Fritsche, phys. status solidi (b) **13**, 487 (1966).
[38] U. De Giovannini, H. Hübener, and A. Rubio, Nano Lett. **16**, 7993 (2016).
[39] C. Cohen-Tannoudji and S. Reynaud, J. Phys. B: At. Mol. Phys. **10**, 345 (1977).
[40] J. Flick, D. M. Welakuh, M. Ruggenthaler, H. Appel, and A. Rubio, ACS Photonics **6**, 2757 (2019).

[41] V. Rokaj, M. Ruggenthaler, F. G. Eich, and A. Rubio, arXiv preprint arXiv:2006.09236 (2021).
[42] M. Durach, A. Rusina, M. F. Kling, and M. I. Stockman, Phys. Rev. Lett. **105**, 086803 (2010).
[43] M. Durach, A. Rusina, M. F. Kling, and M. I. Stockman, Phys. Rev. Lett. **107**, 086602 (2011).
[44] O. Kwon, T. Paasch-Colberg, V. Apalkov, B.-K. Kim, J.-J. Kim, M. I. Stockman, and D. Kim, Sci. Rep. **6**, 21272 (2016).
[45] V. Rokaj, D. M. Welakuh, M. Ruggenthaler, and A. Rubio, J. Phys. B: At., Mol. Opt. Phys. **51**, 034005 (2018).
[46] T. Tamaya and T. Kato, Phys. Rev. B **100**, 081203(R) (2019).
[47] T. Kato, K. Nobusada, and S. Saito, J. Phys. Soc. Jpn. **89**, 024301 (2020).
[48] P. Xia, T. Tamaya, C. Kim, F. Lu, T. Kanai, N. Ishii, J. Itatani, H. Akiyama, and T. Kato, Phys. Rev. B **104**, L121202 (2021).
[49] G. H. Wannier, Phys. Rev. **117**, 432 (1960).
[50] G. H. Wannier, Phys. Rev. **181**, 1364 (1969).
[51] G. N. Watson, *A Treatise on the Theory of Bessel Functions* (Cambridge University Press, 1995).
[52] R. M. Martin, *Electronic Structure: Basic Theory and Practical Methods* (Cambridge University Press, 2004).
[53] B. C. Stuart, M. D. Feit, S. Herman, A. M. Rubenchik, B. W. Shore, and M. D. Perry, Phys. Rev. B **53**, 1749 (1996).
[54] S. Pearl, N. Rotenberg, and H. M. van Driel, Appl. Phys. Lett. **93**, 131102 (2008).
[55] A. D. Bristow, N. Rotenberg, and H. M. van Driel, Appl. Phys. Lett. **90**, 191104 (2007).
[56] D. Reitze, T. Zhang, W. M. Wood, and M. C. Downer, J. Opt. Soc. Am. B **7**, 84 (1990).
[57] T. Sjodin, H. Petek, and H.-L. Dai, Phys. Rev. Lett. **81**, 5664 (1998).
[58] T. F. Boggess, S. C. Moss, I. W. Boyd, and A. L. Smirl, Opt. Lett. **9**, 291 (1984).
[59] E. D. Palik, *Handbook of Optical Constants of Solids* (Academic Press, 1985).
[60] J. Shah, R. F. Leheny, and C. Lin, Solid State Commun. **18**, 1035 (1976).
[61] M. Noda, K. Iida, M. Yamaguchi, T. Yatsui, and K. Nobusada, Phys. Rev. Appl **11**, 044053 (2019).